FISEVIER

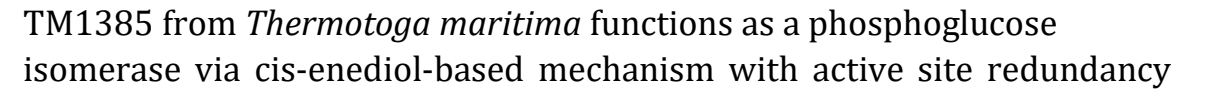
Contents lists available at ScienceDirect

BBA - Proteins and Proteomics

journal homepage: www.elsevier.com/locate/bbapap



Research Paper



Nicole Swope ¹, Katherine E. Lake ¹, Golda H. Barrow ², Daniel Yu, Daniel A. Fox ³, Linda Columbus ^{*}

Department of Chemistry, University of Virginia, Charlottesville, VA, USA



Keywords:
Phosphoglucose isomerase
Thermotoga maritima
Enediol
Enzyme characterization



Phosphoglucose isomerases (PGIs) belong to a class of enzymes that catalyze the reversible isomerization of glucose-6-phosphate to fructose-6-phosphate. PGIs are crucial in glycolysis and gluconeogenesis pathways and proposed as serving additional extracellular functions in eukaryotic organisms. The phosphoglucose isomerase function of TM1385, a previously uncharacterized protein from *Thermotoga maritima*, was hypothesized based on structural similarity to established PGI crystal structures and computational docking. Kinetic and colorimetric assays combined with ¹H nuclear magnetic resonance (NMR) spectroscopy experimentally confirm that TM1385 is a phosphoglucose isomerase (TmPGI). Evidence of solvent exchange in ¹H NMR spectra supports that TmPGI isomerization proceeds through a *cis*-enediol-based mechanism. To determine which amino acid residues are critical for TmPGI catalysis, putative active site residues were mutated with alanine and screened for activity. Results support that E281 is most important for TmPGI formation of the *cis*-enediol intermediate, and the presence of either H310 or K422 may be required for catalysis, similar to previous observations from homologous PGIs. However, only TmPGI E281A/Q415A and H310A/K422A double mutations abolished activity, suggesting that there are redundant catalytic residues, and Q415 may participate in sugar phosphate isomerization upon E281 mutation. Combined, we propose that TmPGI E281 participates directly in the *cis*-enediol intermediate step, and either H310 or K422 may facilitate sugar ring opening and closure.

1. Introduction

Phosphoglucose isomerases (PGIs) represent a class of enzymes responsible for catalyzing the reversible isomerization between glucose-6-phosphate (G6P) and fructose-6-phosphate (F6P) (Fig. 1), a step in the glycolysis and gluconeogenisis pathways [1]. Eukaryotic PGI has additional functions as a "moonlighting protein" when secreted outside of the cell. For example in rabbits, PGI, neuroleukin, autocrine motility factor, and differentiation and maturation mediator all share the same amino acid sequence, but possess different names depending on the protein function, pathway, and location [2]. In humans, mutations of PGI can result in nonspherocytic hemolytic anemia, a genetic disorder in which PGI mutations cause either destabilization of the functional protein dimer and/or active site [2], resulting in red blood cells that prematurely undergo hemolysis [3]. Additionally, serum PGI elevation

can correlate with metastasis in cancer patients [4]. An understanding of the enzymatic function of PGI is important to the study of various biological and clinical applications of this protein.

Mechanistic studies of PGI from human, rabbit, *Pyrococcus furiosus*, and *Thermococcus kodakarensis* have been published [5–8]. While a direct hydride shift PGI mechanism (Fig. S1) has been proposed and supported by structural analysis [9], functional assays and co-crystal structures with PGI inhibitors provide strong evidence for an acid-base catalysis mechanism proceeding through a substrate *cis*-enediol intermediate for the forward and reverse isomerization reaction between G6P and F6P [7,8,10,11]. Proton donation by a PGI residue is thought to be responsible for acid-catalysis that results in the opening and closing of the glucose or fructose ring. A PGI residue is similarly thought to function as a catalytic base to form the *cis*-enediol intermediate [5,10,12,13].

To date, there are over fifty PGI crystal structures reported in the

E-mail address: columbus@virginia.edu (L. Columbus).

 $^{^{}st}$ Corresponding author.

¹ These authors contributed equally.

² Present address: Biocomplexity Institute and Initiative, University of Virginia, Charlottesville, VA, USA

³ Present address: Albemarle Corporation, Baton Rouge, LA, USA

Protein Data Bank (PDB). While most PGIs with available crystal structures have either bound substrates or in vitro kinetics to support their functions, protein TM1385 (PDB ID: 2Q8N) from Thermotoga maritima represents a proposed PGI based solely on the apo structure [14]. TM1385 was crystallized as part of a Joint Center for Structural Genomics (JCSG) initiative to crystallize the *T. maritima* proteome [14], but its putative designation as a PGI and functional mechanism had yet to be confirmed biochemically. Characterization of a thermostable PGI from a deeply-branched organism such as T. maritima (TM1385) [15] may provide insight into PGI evolution, as the sequence is homologous to PGIs spanning eukaryotic, bacterial, and archaeal species (Fig. S2). PGIs derived from several thermophilic bacterial and archaeal species possess bifunctionality and also serve as phosphomannose isomerases (PMIs) [16]. TM1385 therefore requires assessment for PMI bifunctionality. Thermostable PGIs are additionally advantageous for engineering enzymes suitable for use in bioreactors [17], underscoring the technological importance of understanding T. maritima PGI (TM1385; TmPGI).

TmPGI function and mechanism was investigated using kinetic, colorimetric, and ¹H nuclear magnetic resonance (NMR) assays. Compared to PGIs found in other bacterial thermophiles, TmPGI functions solely as a PGI with no dual PMI activity. To identify TmPGI residues critical for catalysis, alanine mutations were introduced at conserved active site residues E281, H310, Q415, and K422. Kinetic and colorimetric assays indicate that E281 is important for TmPGI activity and may be the residue catalyzing formation of the cis-enediol intermediate, supporting previous studies with TmPGI homologs [5,10,12]. However, the catalytic role of E281 can be compensated by other residues such as Q415. Activity assays additionally show that H310, Q415, and K422 mutations reduce activity yet none of the mutations abolish activity. Across functional studies with TmPGI mutants, only E281A/ Q415A and H310A/K422A double mutations were inactive even at high enzyme concentrations. Based on mutations of these neighboring residue pairs, both sides of the TmPGI active site play direct roles in catalysis. Combined, structural and functional analysis of TmPGI suggests that optimal activity is achieved when H310 and K422 are both present to open the sugar ring, and E281 catalyzes the isomerization step.

2. Materials and methods

2.1. TM1385 structure and multiple sequence alignments

Global structure alignments of the TM1385 apo dimer (PDB ID: 2Q8N) and twenty classified PGIs were performed with Chimera [18] (Table S1). Selected PGIs were chosen based on availability of crystal structures in the PDB. To identify conserved residues within the putative PGI active site, a multiple sequence alignment was generated with Expresso [19] and ESPript [20] using amino acid sequences from aligned structures.

2.2. TM1385 mutagenesis, expression, and purification

The pMH1 vector encoding the recombinant TM1385 protein with a N-terminal $6\times$ His fusion tag was obtained from the Joint Center for Structural Genomics. To generate TM1385 with alanine point mutations, PCR using the Polymerase Incomplete Primer Extension (PIPE) method [21] or QuikChange Lightning Site-Directed Mutagenesis kit (Agilent Technologies) was performed with a BioRad C1000 Thermal Cycler. After PCR, *E. coli* Top 10 cells were transformed with the mutagenized plasmid. Supercoiled mutagenized DNA was purified using the QiaPrep Spin Miniprep Kit (Qiagen). Protein sequences were confirmed by Sanger Sequencing (GENEWIZ) with pBAD forward and backward primers.

For protein expression, TM1385 wild-type and mutant plasmids were transformed into HK100 E. coli cells. One liter cultures in LB media supplemented with 100 µg/mL ampicillin were grown in shake flasks at 37 °C, 225 rpm until the OD_{600} reached 0.8–1.0. Protein expression was induced with 0.02% arabinose for four hours at 37 °C, 225 rpm. Cells were harvested by centrifugation at 4000 rpm, 4 $^{\circ}\text{C}$ for 20 min. For lvsis. cells were resuspended in cell lysis buffer (50 mM Tris pH 8.0 and 150 mM NaCl) containing EDTA-free protease inhibitor cocktail (Roche) and passed twice through a Nano DeBEE high pressure homogenizer (BEE International) at 25,000 psi. The lysate containing the soluble recombinant protein was loaded onto 1 mL bed volume of Chelating Sepharose Fast Flow resin (GE Life Sciences) charged with 100 mM CoCl₂ solution. The resin was washed with 20 column volumes (CV) of wash buffer (20 mM phosphate buffer, pH 7.8, 150 mM NaCl and 20 mM imidazole). Protein bound to the resin was eluted with 5 CV of elution buffer (wash buffer supplemented to 600 mM imidazole). Purification performance was monitored with SDS-PAGE analysis. The purified protein from the elution fraction was dialyzed twice at room temperature for 4 h each against 4 L of Buffer A (50 mM Tris, 150 mM NaCl, pH 7.0). Protein concentration was determined by absorbance at 280 nm. For experiments using high TM1385 concentrations, dialyzed samples were concentrated with Amicon filtration devices using a 30,000 Da molecular weight cutoff (Millipore).

2.3. Kinetic assay using coupled Glucose-6-phosphate dehydrogenase

The catalytic isomerization activity of TM1385 was determined spectrophotometrically by NADPH absorbance at 340 nm. The coupled enzyme assay to measure TM1385 activity was adapted from Sigma-Aldrich using glucose-6-phosphate dehydrogenase (G6PDH from *S. cerevisiae*, Sigma-Aldrich) [22] and the substrate fructose-6-phosphate (F6P, Sigma-Aldrich). Assays were performed in Buffer A at room temperature in reactions containing 60 nM TM1385, 4.7 U/mL G6PDH, 10 mM MgCl₂, and 1 mM NADP⁺ with varying F6P concentrations (1–25 mM for wild type, 25–1500 mM for mutants). A protein concentration of 60 nM wild-type TM1385 gave the most linear change in absorbance with saturating F6P concentrations. Coupled assay reactions were carried out in 96-well plates using a 200 µL reaction volume. Absorbance readings were recorded at 340 nm for 30 s with the Epoch microplate

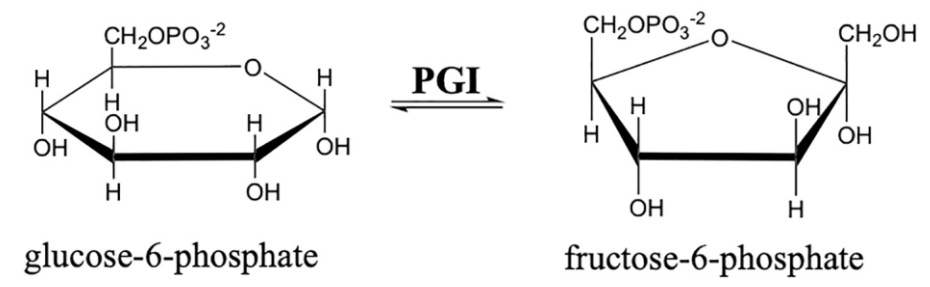


Fig. 1. Phosphoglucose isomerases (PGIs) catalyze glucose-6-phosphate and fructose-6-phosphate isomerization. Glucose-6-phosphate (G6P) undergoes isomerization to fructose-6-phosphate (F6P) in a reversible process.

spectrophotometer (BioTek) to quantify NADPH formation upon successful G6PDH reaction with G6P produced by TM1385. The change in NADPH concentration was determined by dividing the change in absorbance at 340 nm by the extinction coefficient of NADPH (6220 M⁻¹ cm⁻¹) and path length within the microplate (0.5 cm) to obtain TM1385 catalysis rates. Mutant TM1385 kinetics assays required high concentrations of commercially-available F6P to observe activity, resulting in G6P impurities at a concentration sufficient for G6PDH catalysis. Therefore, controls were run with excess NADP+, G6PDH, 10 mM MgCl₂, and 1500 mM F6P, the maximum F6P concentration used in mutant kinetics studies, prior to mutant TM1385 addition. These studies resulted in plate reader absorbance values beyond the linear range of the instrument, Thus, F6P reactions without TM1385 for each F6P concentration were used in background subtraction for determining reaction rates. Michaelis-Menten kinetic parameters were generated based on rate of NADPH formation (V) versus F6P concentration ([F6P]) and fit to Eq. 1 in Origin Pro software:

$$V = \frac{V_{\text{max}}[F6P]}{K_M + [F6P]} \tag{1}$$

Phosphogluconate inhibition assays were performed using the G6PDH-coupled assay conditions described for F6P substrate. Michaelis-Menten curves were generated from reacting 1.0 mM 6-phosphogluconic acid (6P-gluconate) with 60 nM of wild-type TM1385. To exclude the possibility of 6P-gluconate acting primarily on the G6PDH coupling enzyme, assays were conducted with the G6PDH-catalyzed conversion of G6P to 6-phosphoglucolactone using 0.6 U of G6PDH in the absence of TM1385. The inhibition constant (Ki) of 6P-gluconate was determined from the concentration of 6P-gluconate (I), apparent $K_{\rm M}$ with 6P-gluconate, and $K_{\rm M}$ (Eq. 1) according to the equation for a competitive inhibitor:

$$K_{i} = \frac{[I]}{\frac{K_{M,apparent}}{K_{M}} - 1}$$
 (2)

2.4. NMR spectroscopy

All NMR experiments were performed on a Bruker 600 MHz spectrometer at 25 $^{\circ}\text{C}$ using 500 μL sample volumes. Samples containing 60 nM TM1385, 10 mM substrate (G6P or F6P), and Buffer A in 90% $\text{H}_2\text{O}/10\%$ D2O and 15% H2O/85% D2O were prepared and incubated for 2 h at 60 $^{\circ}\text{C}$. Incubation at 60 $^{\circ}\text{C}$ allowed efficient TM1385 equilibration of substrate, likely owing to the enzyme's native thermophilic environment. One-dimensional ^{1}H NMR spectra were recorded using water presaturation with composite pulses (*zgcppr* pulse sequence) and 16 transients. The NMR spectra of substrate samples without TM1385 were used to assign the proton resonances of G6P and F6P and serve as negative controls (Figs. S1 and S2).

2.5. TM1385 computational docking with linear G6P substrate

The SwissDock server [23] was utilized to dock linear G6P ligand to the TM1385 structure. All non-standard ligands (nonaethylene glycol, H_2O , SO_4^{2-} , Cl^-) as well as chain C, which does not contribute to an active site, were removed from the PDB file prior to docking analysis. Location parameters were unchanged to prevent biased docking to the putative active site. Docking type was set to accurate, a setting allowing for the most accurate docking results at the expense of speed. Flexibility of ligand side chains was allowed up to 3.0 Å. From the SwissDock output, resulting ligand poses were ranked according to the lowest Gibbs free energy, which allows for a non-biased ranking system of ligand positions and sites that G6P is most likely to be interacting with TM1385. The 15 docked G6P poses with lowest Gibbs free energy scores were further analyzed to establish presence in the active site and relative orientation of the ligand phosphate group. To compare docking results with available PGI co-crystal structures containing linear G6P, TM1385

with docked G6P was structurally aligned with the bifunctional PGI/PMI from *Pyrobaculum aerophilum* [16] (PaPGI/PMI, PDB ID: 1X9I [24]). Root-mean-square deviation (RMSD) calculations were performed between the SwissDock poses and aligned G6P from the PaPGI/PMI cocrystal structure.

2.6. Colorimetric (Seliwanoff) assay

End-point assays to determine F6P and G6P substrate equilibria from TM1385 catalysis were performed in 96-well plates at 100 µL volumes. Reactions were tested with the low concentration of TM1385 used in G6PDH-coupled assays (60 nM) or amplified TM1385 concentrations (2.3 µM), 10 mM substrate (F6P, G6P, or mannose-6-phosphate [M6P]) and Buffer A. Equilibration was achieved by incubating reactions for 2 h at 60 °C. Wells without TmPGI but known F6P concentrations (0, 2, 4, 6, 8, and 10 mM) were included on the same plate to generate a standard curve. 10 mM G6P and M6P controls in Buffer A ensured that the presence of aldose sugars did not interfere with quantification of F6P. After the incubation period, 100 µL of Seliwanoff's reagent (4 N HCl, 0.1% (w/v) resorcinol) was added to samples. A microplate seal (VWR) was applied, and the plate was placed on glass supports in a 100 °C convection oven for 20 min. Upon incubation at 100 °C, a red product forms with reaction of F6P and Seliwanoff's reagent [25]. Following the incubation period, the microplate seal was removed, and absorbances were measured at 480 nm using the iMark microplate absorbance reader (BioRad). F6P concentrations in TmPGI reactions were determined by the F6P standard curve, and G6P (or M6P) concentrations were determined from subtracting the final F6P concentration from the initial F6P concentration (10 mM).

3. Results and discussion

3.1. Structure alignments to homologous PGIs and substrate docking support TM1385 PGI function

To compare the TM1385 protein structure to classified PGIs, structure alignments were generated using twenty PGI crystal structures spanning bacterial, eukaryotic, and archaeal species (Table S1). Aligning PGIs with known structure and function allowed for comparison of homologous PGI active site residues to conserved residues within the TM1385 sequence (Fig. S2). A representative structure alignment of TM1385 with an archaeal PGI homolog possessing dual phosphomannose (PMI) functionality from *Pyrobaculum aerophilum* [16] (PaPGI/PMI, PDB ID: 1X9I [24]) is shown in Fig. 2. PaPGI/PMI was selected for final rendering due to similarity to the TM1385 structure, identification of active site residues, co-crystallized linear G6P in the active site, and thermophilic species origin.

Most of the PaPGI/PMI active site residues are highly or strictly conserved across PGI homologs and TM1385. A multiple sequence alignment with TM1385 and known PGIs demonstrates that S77, S136, T141, R198, E281, H310, and K422 are strictly conserved, while position 138 is highly conserved as a serine or threonine. Positions 197 and 415 are glycine and glutamine, respectively, among aligned PGIs except for PaPGI/PMI (Fig. S2). Furthermore, conserved residues within the TM1385 crystal structure show a remarkable similarity to the PaPGI/ PMI active site architecture in Fig. 2. We thus propose that for TM1385. residues S77, S136, S138, T141, G197, R198, E281, Q415, and K422 in the first subunit and H310 in the second subunit form the putative active site for PGI function. Homologous residues to E281, H310, and K422 have all been proposed as serving direct roles in PGI catalysis [11,12]. R198 and Q415 are thought to stabilize the negative charge of E281 and/or cis-enediol(ate) intermediate and participate in hydrogen bonding with the substrate, respectively [12,26]. The hydroxyl groups of serine and threonine residues have previously been reported to stabilize the substrate phosphate group [27]. Combined, the structure and sequence alignments of TM1385 with known PGIs lends convincing

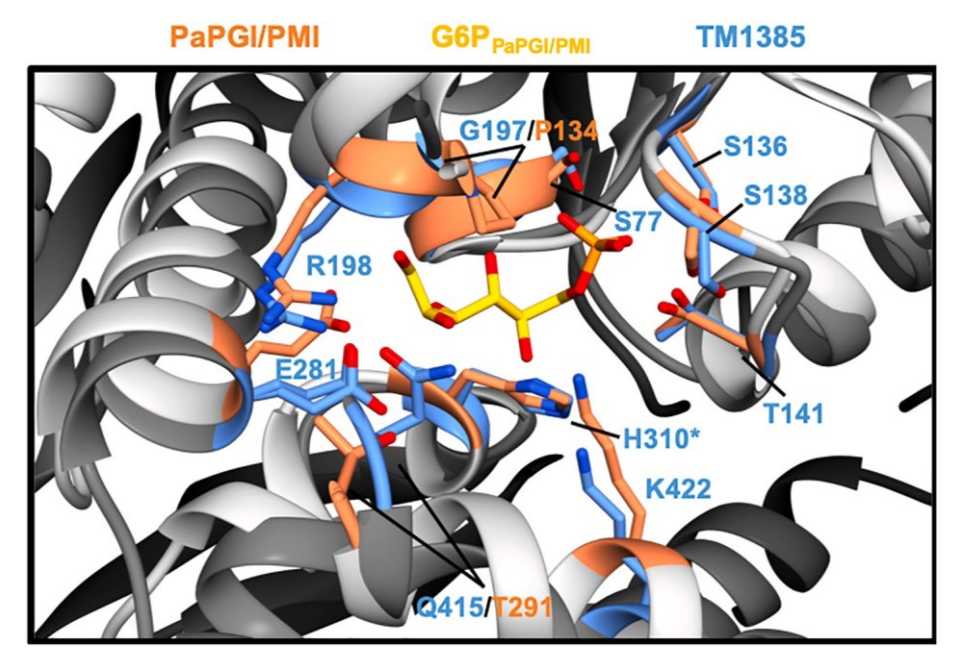


Fig. 2. Structural evidence for TM1385 phosphoglucose isomerase function based on alignment with *Pyrobaculum aerophilum* PGI/PMI. TM1385 (PDB ID: 2Q8N, dark gray and blue) and PaPGI/PMI cocrystallized with glucose-6-phosphate (G6P, yellow) substrate (PDB ID:1X9I [24], light gray and coral) were structurally aligned using Chimera software [17]. Conserved PGI active site residues within the TM1385 sequence are labeled with TM1385 residue numbers, with non-conserved residues labeled for both proteins. Asterisk denotes a residue located in the second subunit.

support that TM1385 is in the phosphoglucose isomerase family.

3.2. TM1385 (TmPGI) catalyzes fructose-6-phosphate to glucose-6-phosphate isomerization

To test the proposed PGI function of TM1385, a coupled enzymatic assay with glucose-6-phosphate dehydrogenase (G6PDH) [22] was designed to measure TM1385 activity in the F6P to G6P isomerization direction. Upon F6P isomerization to G6P, G6PDH converts G6P to 6-phosphogluconolactone using NADP as a cofactor. Thus, formation of NADPH was measured by spectrophotometry at 340 nm. Increasing F6P concentration resulted in increasing reaction rates, following Michaelis Menten kinetics, with a $\rm K_M$ of 0.31 mM and $\rm k_{cat}$ of 17.4 s⁻¹ (Fig. 3;

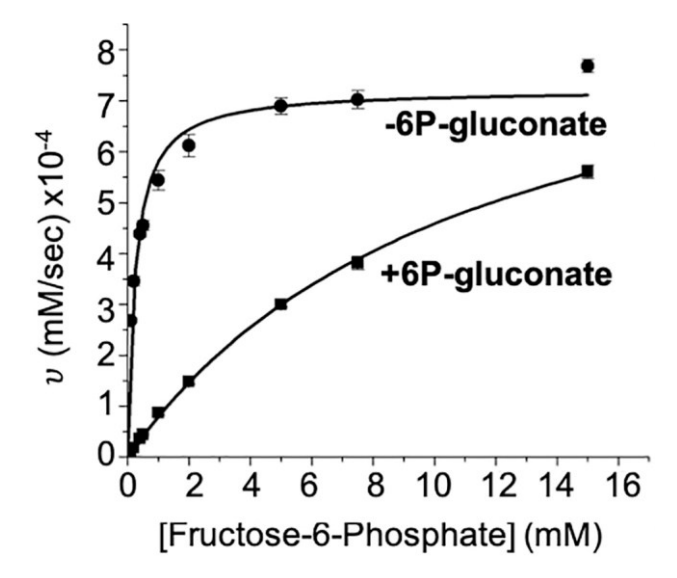


Fig. 3. Steady-state kinetics using glucose-6-phosphate dehydrogenase coupling enzyme confirms PGI function of TM1385. TM1385 (TmPGI) catalysis was assayed based on F6P to G6P isomerization coupled to glucose-6-phosphate dehydrogenase (G6PDH) activity. Reaction rates were measured based on formation of NADPH (mM) for 30 s. Addition of the known competitive PGI inhibitor 6P-gluconate decreases TmPGI activity. Error bars represent the standard deviation of triplicates.

Table 1Michaelis-Menten kinetic parameters of TmPGI variants with fructose-6-phosphate (G6PDH-Coupled Assay).

TmPGI Variant	K _M (mM)	$k_{cat} (s^{-1})$	$k_{cat}/K_M (mM^{-1} s^{-1})$
WT	0.31 ± 0.03	17.4 ± 0.4	58.8 ± 6.2
E281S	NA ^a	NA	NA
E281A	NA	NA	NA
H310A Q415A	$233 \pm 100 \\ 376 \pm 150$	$65 \pm 12 \\ 70 \pm 11$	$\begin{array}{c} 0.3 \; \pm \; 0.2 \\ 0.2 \; \pm \; 0.1 \end{array}$
K422A	478 ± 180	86 ± 13	0.2 ± 0.1
E281A/H310A	NA	NA	NA
E281A/Q415A	NA	NA	NA
H310A/K422A	NA	NA	NA

^a No activity observed.

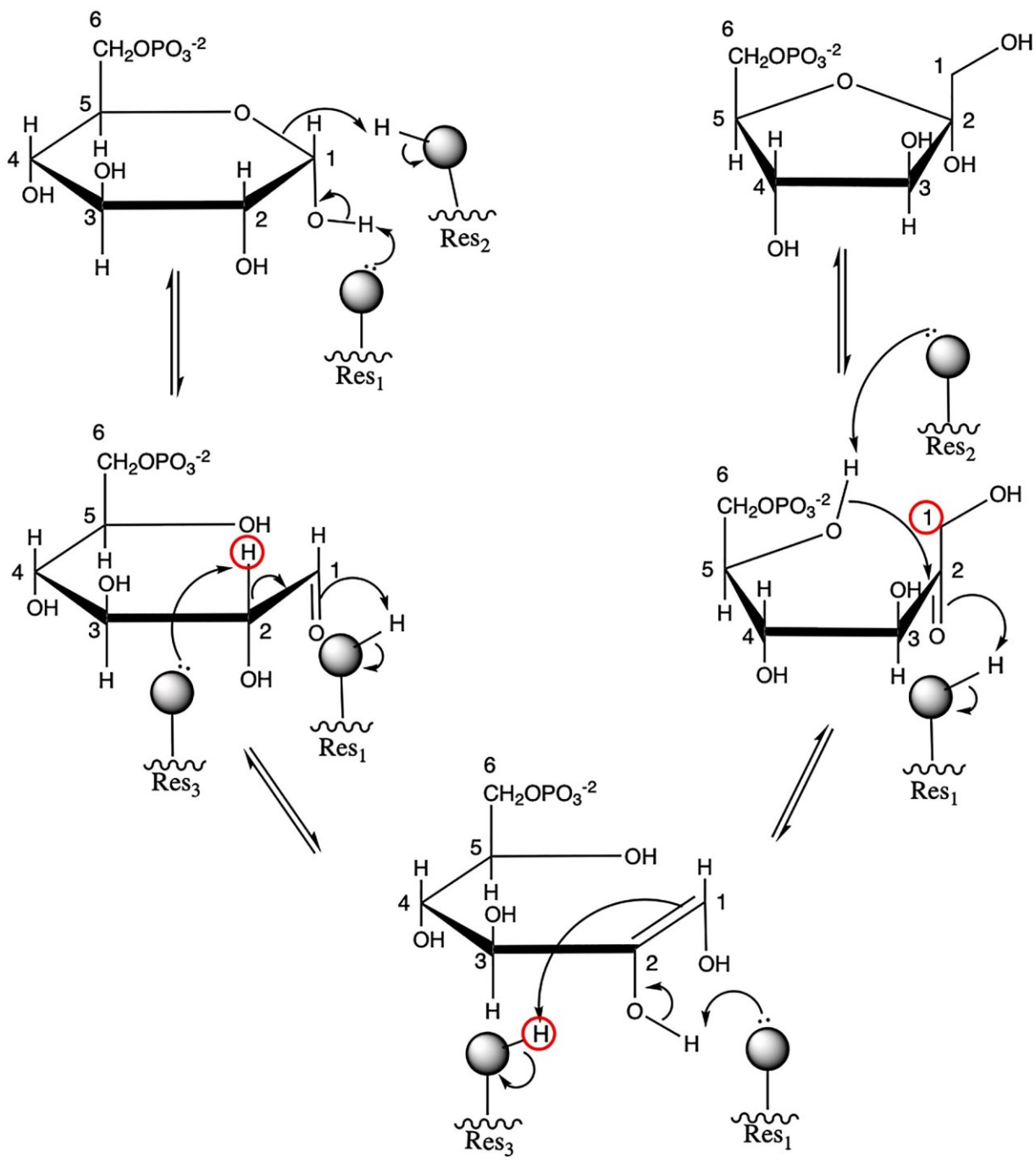
Table 1), confirming that TM1385 is a PGI (TmPGI). The K_M is similar to reported values for *Pyrobaculum aerophilum* (0.30 mM) [16], *Mycobacterium tuberculosis* (0.27 mM) [28], and *Carassius auratus* (0.36 mM) [29], while the k_{cat} is most similar to those reported for *Pyrococcus furiosus* (8.4 s⁻¹) [7] and *Carassius auratus* (18.0 s⁻¹) [29]. Furthermore, addition of the known PGI inhibitor 6P-gluconate [30] decreased TmPGI activity (K_L 44 μ M). 6P-gluconate did not inhibit the G6PDH coupling enzyme with G6P substrate.

3.3. TmPGI catalysis proceeds through a cis-enediol intermediate pathway

Kinetic studies may be used to designate TM1385 as a PGI; however, kinetics alone do not give information on the mechanism of accomplishing substrate isomerization. There are two predominant mechanisms for substrate isomerization: (1) a direct hydride shift, proposed for metal-dependent PGIs (Fig. S1) [9] or (2) a mechanism involving a *cis*-enediol intermediate (Fig. 4) [7]. The *cis*-enediol mechanism was previously demonstrated for both metal-dependent and metal-independent PGIs [7–10]. In the direct hydride shift mechanism, a hydride ion is removed from carbon 2 (C2) of G6P and directly donated to carbon 1 (C1) in order to form F6P without exchange with the solvent. In the *cis*-enediol mechanism, a residue in the PGI enzyme active site acts as a base catalyst to remove a proton from C2 of G6P, and the substrate forms a *cis*-enediol intermediate. The proton that is removed by the PGI base catalyst may exchange with protons from the solvent before being

glucose-6-phosphate

fructose-6-phosphate



cis-enediol intermediate

Fig. 4. TmPGI proton exchange is facilitated by catalytic active site residues proposed in the *cis*-enediol-based mechanism. G6P ring opening is the first step in the hypothesized *cis*-enediol mechanism for TmPGI, initiated by residue 1 (Res₁). Residue 2 (Res₂) donates a proton to the oxygen atom in the sugar ring to form a hydroxyl at carbon 5, facilitating a linearized substrate conformation. The *cis*-enediol intermediate occurs upon proton abstraction (red circle) by residue 3 (Res₃), with Res₁ accepting the leaving proton as part of an acid/base residue pair with Res₃. Isomerization to linear F6P is complete after a proton is donated back to the substrate C1 position (red circle) by Res₃. Finally, Res₁ and Res₂ return the substrate to its cyclic form. Proposed mechanism is based on previous work from [5–7,10].

donated to C1 to form the product [7]. Proton exchange between TmPGI residues and substrate is demonstrated in Fig. 4.

In order to distinguish between these two mechanisms for the TmPGI reaction, NMR experiments were used to determine whether the proton transferred from C2 to C1 of the sugar substrate is able to exchange with solvent protons during the course of the reaction [7,8]. The $^1\mathrm{H}$ NMR

spectra of the sugar-phosphate substrates after reaction with PGI may be compared when the reaction takes place in a solvent containing mostly H_2O or D_2O . When D_2O solvent is used, deuteron incorporation may occur after formation of the \emph{cis} -enediol intermediate, when the proton removed by a TmPGI residue exchanges with a deuteron of the solvent (as D_2O). A deuteron is then incorporated into the substrate to complete

the isomerization. If deuterons are incorporated into the sugar during the PGI reaction in high D2O solvent (at either of the H1 positions in F6P or at the H1 or H2 position in G6P), a decrease in intensity or disappearance of the resonances corresponding to these protons in a ¹H NMR spectrum will be observed (Fig. S3A). Conversely, because the direct hydride shift mechanism does not allow for the transferred hydrogen atom to exchange with the solvent, a decrease in resonance intensity corresponding to proton positions in the substrate that are involved in the reaction will not be observed (Fig. S3B). Reactions performed in the absence of a bivalent metal source with G6P substrate and TmPGI in 10% and 85% D_2O (Fig. 5) show that the G6P H1- α , H1- β , H2- β , and H3 resonances disappear or largely decrease, supporting that TmPGI catalysis proceeds through a cis-enediol intermediate. The NMR results demonstrate that there is no bivalent metal requirement for TmPGI activity, agreeing with sequence similarities to metal-independent PGIs (Fig. S1).

3.4. Computational docking to investigate crucial residues for TmPGI function

As the TmPGI crystal structure does not contain bound substrate, computational docking between the TmPGI structure and linear G6P substrate was performed via the SwissDock server [23] to identify which residues may be important for substrate binding and/or catalysis via a cis-enediol mechanism. PGIs have been co-crystalized with both linear and cyclic forms of substrate; for the purpose of identifying the residues involved in the proton transfer step, the linear sugar was used in the docking procedures. The 15 docked G6P poses with the lowest Gibbs free energy ranged from _9.41 to _ 9.73 kcal/mol and were classified based on active site or surface locations (Table S2). Among the 15 poses with the lowest Gibbs free energy, 12 total poses are found in the two different active sites of the TmPGI dimer (Fig. 6A and Fig. S6), and 3 poses are on the exterior surface of the protein. The most noticeable difference between G6P docking results was relative orientation of the substrate phosphate group. Within the lowest-energy G6P poses located in active sites, 6 are found with the G6P phosphate group angled toward TmPGI residue R198 (Fig. 6B). The remaining 6 poses have a phosphate orientation near TmPGI residue T141 (Fig. 6C), which is a similar G6P conformation compared to the PaPGI/PMI co-crystal structure [24] (Fig. S7B). All PGIs co-crystallized with sugar-phosphate substrates to date closely associate the phosphate group with homologous threonine residues, which suggests the substrate orientation in Fig. 6B is not likely. The RMSD between aligned G6P from PaPGI/PMI and docked poses is 4.7 <u>Q</u>.4 Å (Table S2).

Although PGI crystal structures with substrates and inhibitors have allowed detailed analysis of active site residues, different structural interpretations have led to the identification of various residues that could participate in the *cis*-enediol reaction mechanism. The crystal structures of rabbit PGI with various substrates suggest that the enzyme catalyzes both the ring opening and proton transfer steps in the mechanism [6]. Substrate ring opening and closing may occur with residues analogous to H310 [10,12,13,31] or K422 [5,10–12,31], both of which can act as an acid/base catalyst according to the mechanism in Fig. 4. Importantly, the positive charge of K422 may stabilize the phosphate group of the substrate and orient the molecule within the active site without playing a direct role in catalysis [10].

H310 has additionally been proposed to act as a base catalyst that forms the *cis*-enediol substrate intermediate [2,26,31]. A separate hypothesis for *cis*-enediol formation is that E281 instead acts as the base catalyst [5,10,12,32], perhaps forming an acid/base pair with H310 [26,31] that increases reaction efficiency. H310, E281, and K422 are all strictly conserved across the PGI family, highlighting their potential importance for PGI function. Q415 represents another highly conserved residue adjacent to E281 that could act as a TmPGI base catalyst. However, the glutamine residue would likely be a weaker proton acceptor than the nearby glutamate because the amide group of a

glutamine cannot readily participate in acid/base chemistry.

Distances of G6P substrate to E281, H310, Q415, and K422 are all less than 5 Å in the PaPGI/PMI crystal structure, suggesting crucial catalytic and/or stabilization roles for these residues. However, the top 15 docked G6P poses in the TmPGI crystal structure contain modified substrate orientations from PaPGI/PMI, resulting in longer distances (~3.5–7.0 Å) between proposed catalytic residues and docked substrate. E281 and Q415 remain less than 5 Å to docked G6P, while H310 and K422 are positioned ~5–7 Å away. Longer distances observed between TmPGI and docked G6P does not preclude E281, H310, Q415, and K422 from catalytic roles, as conformational changes not captured by docking may occur in the active site during ligand binding and/or catalysis. For example, two induced-fit conformational rearrangement steps are proposed for the rabbit PGI (rPGI) cis-enediol mechanism [10]. Future studies with TmPGI co-crystallized with cyclic and linear forms of F6P and/or G6P will be needed to confirm similar conformational rearrangements during TmPGI catalysis.

3.5. Functional analysis of proposed TmPGI catalytic residues

To establish TmPGI residues crucial for G6P/F6P isomerization based on activity, the G6PDH-coupled assay was performed with E281A, H310A, Q415A, and K422A TmPGI mutants. Steady-state kinetic parameters of each mutant were determined from fitting reaction rates to Eq. 1 and then compared with wild-type TmPGI (Table 1). An additional E281S mutation was made, as we hypothesized that the hydroxyl group may suffice as a base catalyst if the side chain remains near C1 and C2 substrate atoms.

All E281 mutations abolished TmPGI activity, suggesting that the conserved glutamate residue at this position is required for F6P isomerization (Fig. 7). In contrast, H310A, Q415A, and K422A exhibited low catalytic efficiency. Rather than acting as a base catalyst in the isomerization step, the primary role of Q415 is instead proposed as positioning E281 [12] or the substrate [5,26,31] within the active site. As either H310 or K422 could open or close the substrate ring (Fig. 7), it is possible that these residues can compensate for each other in the event of a mutation. In support of H310 and K422 acting in compensatory roles, mutating both residues to alanine (H310A/K422A) resulted in no activity (Table 1). However, the H310A/K422A double mutation, along with the E281A/Q415A double mutation, may destabilize the active site and subsequent protein fold, which would similarly lead to loss of function. Commercially-available F6P contains 2% G6P impurity, making TmPGI mutant assay conditions and background subtraction for the G6PDH-coupled reaction an arduous task with the high F6P concentrations required for turnover by mutants. Difficulty controlling for G6P impurities likely resulted in the large errors associated with steadystate kinetic parameters.

The G6PDH-coupled assay allows TmPGI functional assessment in the reverse (F6P to G6P), but not forward, reaction. Furthermore, we wished to develop a faster approach to determine general functionality of each TmPGI mutant based on final substrate equilibria without relying on a coupling enzyme. The colorimetric Seliwanoff assay commonly used to distinguish ketose and aldose sugars [33] was adapted to measure relative percentages of F6P (ketose sugar) and G6P (aldose sugar) after incubation with TmPGI variants. The Seliwanoff assay may also be used to screen PGIs for dual phosphomannose isomerase (PMI) activity in which M6P (aldose sugar) is converted to F6P. M6P substrate did not form F6P in any assays performed in this study, demonstrating that TmPGI does not possess dual PMI activity. Bifunctional PGI/PMI activity in PaPGI/PMI is attributed to T291 (Fig. 2), which is a glutamine residue (Q415) in TmPGI and conventional PGIs [24].

Overall, the trends in TmPGI function assayed by the Seliwanoff method (Table 2) generally agreed with the G6PDH-coupling assay. However, both E281A and E281S had activity at the high enzyme concentrations used in the assay (compared to the coupled kinetic assay),

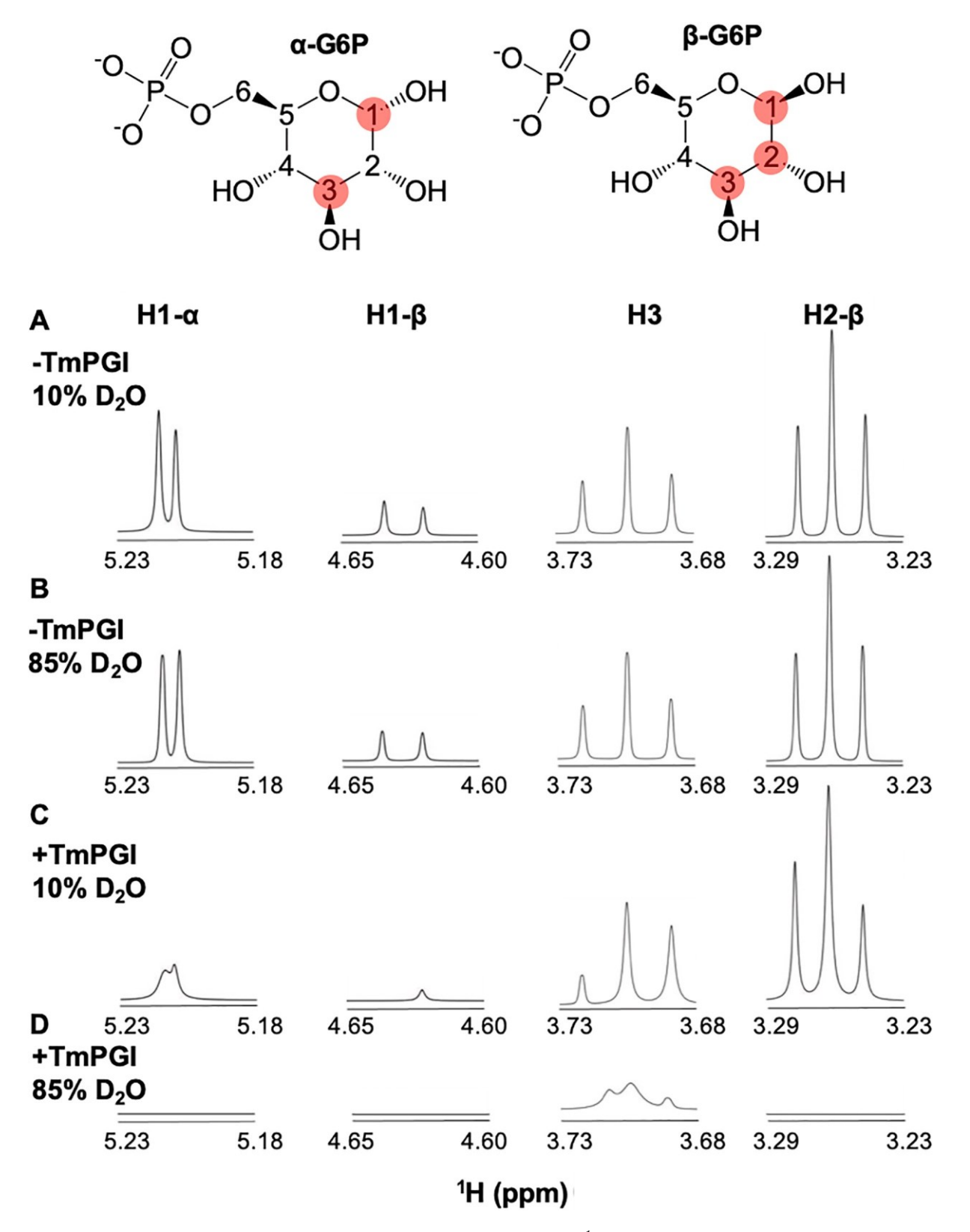


Fig. 5. TmPGI catalyzes G6P to F6P isomerization via a *cis*-enediol intermediate. Experimental 1D 1 H NMR spectra of (A) G6P in 10% D₂O, (B) G6P in 85% D₂O, (C) TmPGI and G6P in 10% D₂O and (D) TmPGI and G6P in 85% D₂O. G6P α and β anomers are both present and produce unique 1 H NMR signals. Loss of G6P H1-α, H1-β, H2-β, and H3 signals in reactions with TmPGI and 85% D₂O solvent indicates that TmPGI catalyzes G6P and F6P isomerization through the *cis*-enediol intermediate pathway. Corresponding protons are labeled on the G6P anomer structures. The H3 resonance could not be assigned to a specific anomer (Fig. S4).

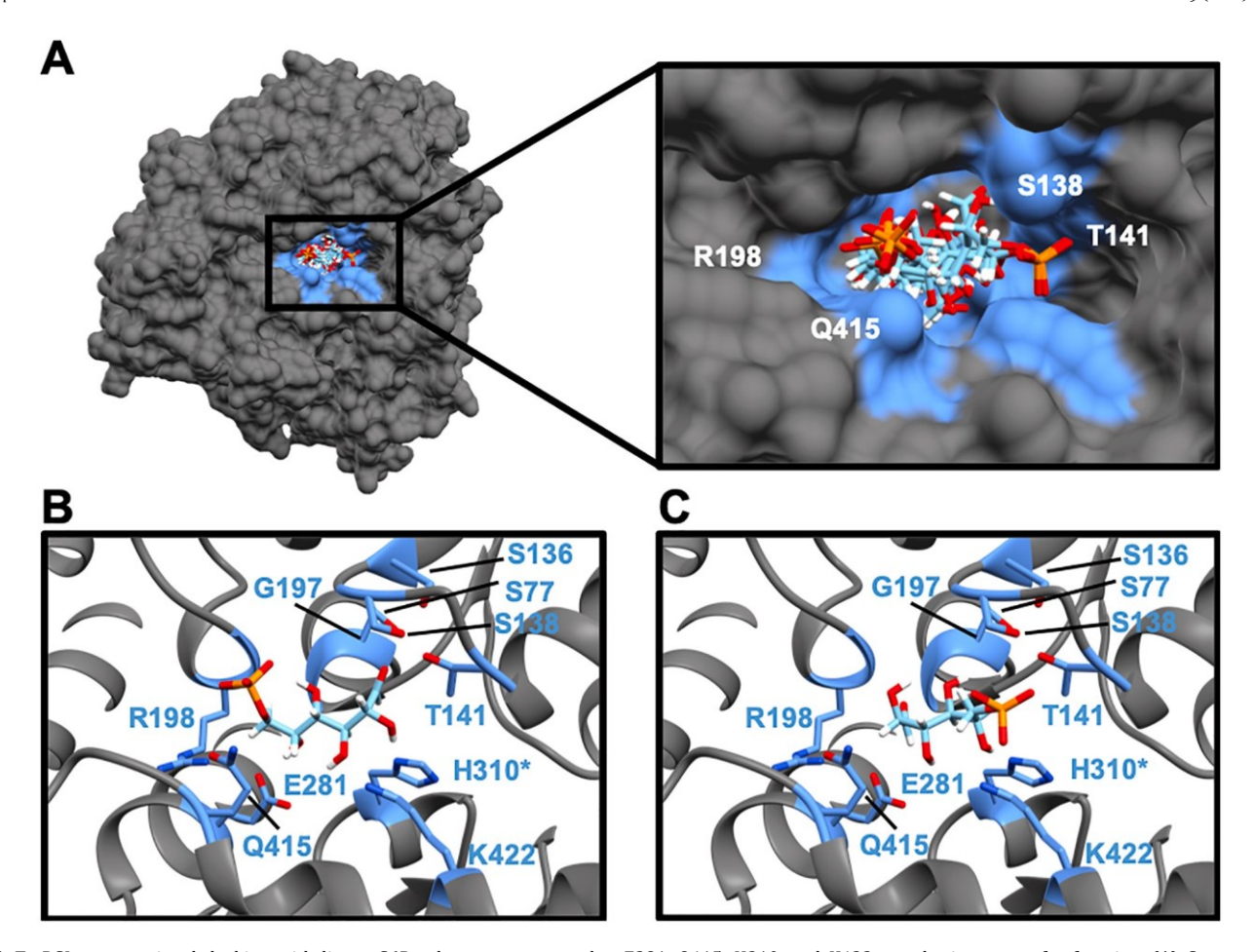


Fig. 6. TmPGI computational docking with linear G6P substrate supports that E281, Q415, H310, and K422 may be important for function. (A) Computational docking with SwissDock [23] was performed with the apo TmPGI crystal structure (dark gray) and linear G6P (cyan sticks). The substrate binding pocket agrees well with the location of proposed active site residues from Fig. 2, highlighted in light blue on the TmPGI surface representation. Eight of the 15 ligand poses with the lowest Gibbs free energy are found in one active site of the TmPGI dimer (shown), and 4 poses are found in the other active site (Fig. S6). The 8 ligand poses shown are superimposed, with S138, T141, R198, and Q415 labeled on the active site to clarify ligand orientation. Docked poses differed based on orientation of the phosphate group in the active site, demonstrated in cartoon representations for (B) and (C). Docked G6P in panel B represents the pose with the lowest Gibbs free energy (-9.73 kcal/mol), while the pose in panel C has a Gibbs free energy of -9.58 kcal/mol.

indicating that E281 is important but not essential for TmPGI activity. Activity detected in the Seliwanoff assay but not the coupled assays suggests that Q415 or another neighboring residue may facilitate TmPGI residual activity in the event of E281 mutation (Fig. 7). Q415 would not typically participate in acid/base chemistry in this way; however, asparagine or glutamine amide side chains are capable of tautomerizing to an imidic acid form if a suitable proton network is stabilized within the active site (Fig. S8) [34]. The pKa for nitrogen protonation/deprotonation in the imidic acid form is estimated between 4.5 and 7.5 [35,36], which allows the nitrogen atom to participate in acid/base chemistry (Fig. 7). TmPGI E281 mutants showing activity only at high enzyme concentrations is recapitulated in the proposed acid/base pair mutant E281A/H310A. The partial function of the E281A/H310A mutant supports the presence of compensatory residues in the TmPGI active site. However, TmPGI function was abolished in both E281A/ Q415A and H310A/K422A based on both G6PDH-coupled and Seliwanoff assays. Combined, the G6PDH-coupled and Seliwanoff assays indicate that E281 and H310 may be compensated by Q415 and K422, respectively, in the event of mutations (Fig. 7). Mutation of both residues in either pair leads to loss of TmPGI function. Suboptimal catalysis in all mutants is indicated by failure to reach the equilibrium condition of F6P to G6P (30% F6P, 70% G6P).

4. Conclusions

In summary, kinetic and colorimetric assays confirm that TM1385 from T. maritima functions as a PGI (now TmPGI). The TmPGI reaction mechanism proceeds through a cis-enediol intermediate, similar to experimental observations based on homologous PGIs with known crystal structures. TmPGI E281 is important for enzyme function and is likely the residue facilitating substrate isomerization in the cis-enediol mechanism. However, Q415 is proposed to position E281 or the substrate in the TmPGI active site and could act as a base catalyst in the absence of E281. H310 or K422 could catalyze ring opening/closing of G6P and F6P, and mutation of one residue may be compensated by the other. Mutation of H310 and K422 simultaneously abolishes TmPGI function, supporting the hypothesis that either H310 or K422 facilitate conversion between ring and linear substrate forms. Future cocrystallization efforts with substrate and/or inhibitors are required to definitively assign the roles of TmPGI active site residues, which could be supplemented by investigating the mechanism stereochemistry [7-10,32]. Finally, TmPGI activity persisting through multiple muta-tions of key active site residues highlights the robustness of the PGI enzyme class and may provide insight into how PGI operates in diverse settings as well as functions, both inside and outside of the cell.

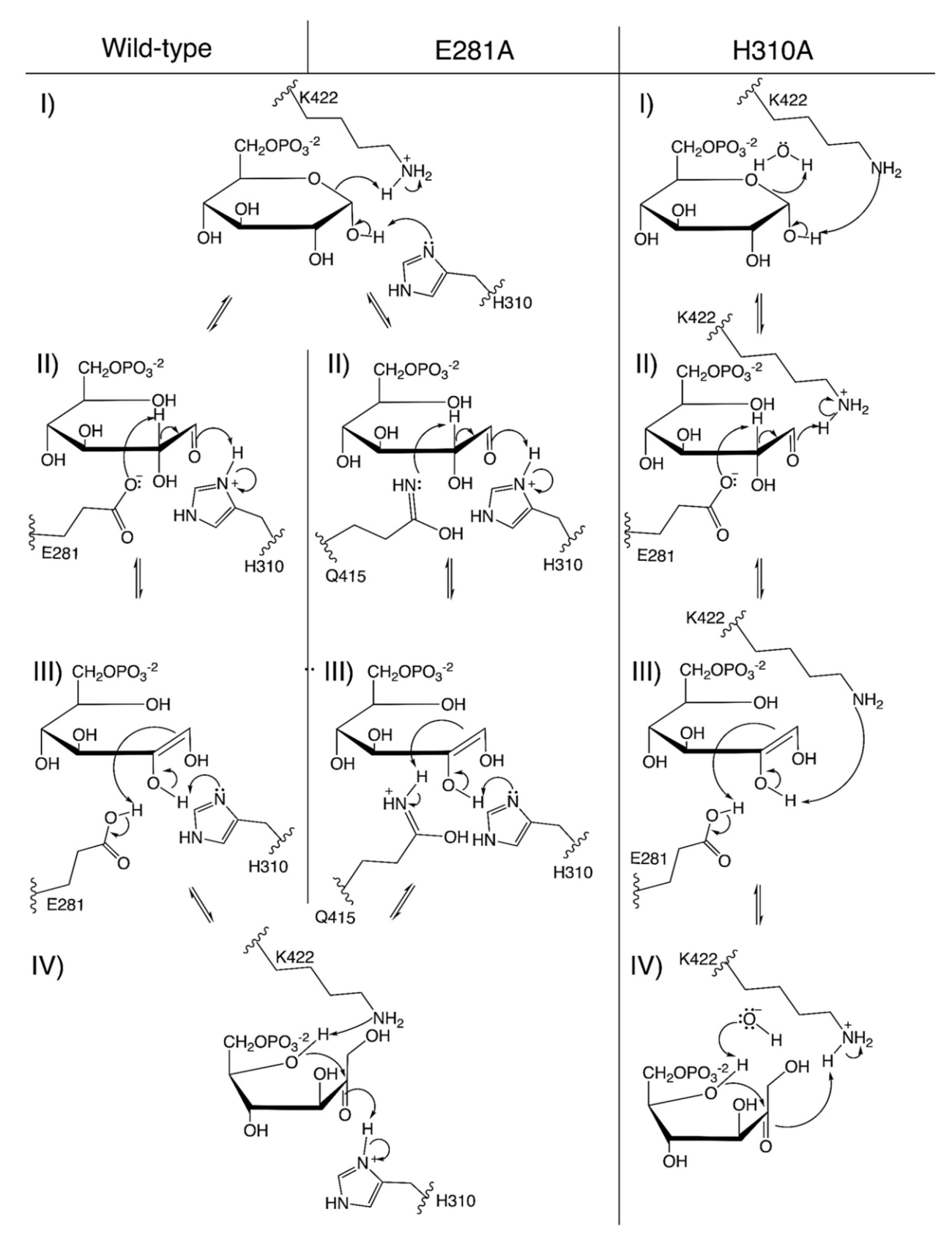


Fig. 7. Summary of TmPGI catalysis and proposed compensatory residue functions. Proposed isomerization mechanisms are shown for wild-type, E281A, and H310A TmPGI variants. Arrows indicate proton exchange between substrate and TmPGI residues/water in I) ring-opening, II) *cis*-enediol formation, III) isomerization, and IV) ring closure. Detailed electron flow of Q415 tautomerization may be referenced in Fig. S8.

 Table 2

 Substrate equilibria of TmPGI variants with F6P substrate (Seliwanoff Assay).

TmPGI Variant ^a	% F6P	% G6P
WT	30	70
E281S	64	36
E281A	55	45
H310A	47	53
Q415A	36	64
K422A	51	49
E281A/H310A	60	40
E281A/Q415A	100	0
H310A/K422A	100	0

 $^{^{\}rm a}$ Results shown are based on 40× TmPGI concentration relative to G6PDH-coupled assays.

Declaration of Competing Interest

The authors declare that they have no conflict of interest with the contents of this article.

Acknowledgments

The authors are grateful to the following individuals for help with the initial characterization of TM1385 as a PGI: Taylor Koerner, Jing Liu, Sun Young Park, Robert Schenck, Amanda Taylor, Ryan Lo, Carol Price, and Cameron Mura. This work was supported by the NSF (MCB 1817735 to L.C.; DDGE 1315231 to N.S.), the NIH (T32 GM008715 to N.S.), and the Double Hoo Research Grant funded by the Jefferson Trust at the University of Virginia (K.L. and N.S.).

Appendix A. Supplementary data

Supplementary data to this article can be found online at https://doi.org/10.1016/j.bbapap.2021.140602.

References

- [1] A. Achari, et al., Glucose 6 phosphate isomerase, Philos. Trans. Royal Soc. Lond. B Biol. Sci. 293 (1063) (1981) 145–157.
- [2] C.J. Jeffery, et al., Crystal structure of rabbit phosphoglucose isomerase, a glycolytic enzyme that moonlights as neuroleukin, autocrine motility factor, and differentiation mediator, Biochemistry 39 (5) (2000) 955–964.
- [3] A. Repiso, et al., Glucose phosphate isomerase deficiency: enzymatic and familial characterization of Arg346His mutation, Biochim. Biophys. Acta (BBA) - Mol. Basis Dis. 1740 (3) (2005) 467–471.
- [4] T. Funasaka, et al., Down-regulation of phosphoglucose isomerase/autocrine motility factor results in mesenchymal-to-epithelial transition of human lung fibrosarcoma cells, Cancer Res. 67 (9) (2007) 4236.
- [5] J. Read, et al., The crystal structure of human phosphoglucose isomerase at 1.6 Å resolution: implications for catalytic mechanism, cytokine activity and haemolytic anaemia, J. Mol. Biol. 309 (2) (2001) 447–463.
- [6] J.H. Lee, C.J. Jeffery, The crystal structure of rabbit phosphoglucose isomerase complexed with D-sorbitol-6-phosphate, an analog of the open chain form of Dglucose-6-phosphate, Protein Sci. 14 (3) (2005) 727–734.
- [7] J.M. Berrisford, et al., Evidence supporting a cis-enediol-based mechanism for Pyrococcus furiosus Phosphoglucose isomerase, J. Mol. Biol. 358 (5) (2006) 1353–1366.
- [8] S.N. Abbas, et al., NMR studies on mechanism of isomerisation of fructose 6-phosphate to glucose 6-phosphate catalysed by phosphoglucose isomerase from Thermococcus kodakarensis, Bioorg. Chem. 66 (2016) 41–45.
- [9] M.K. Swan, et al., Structural evidence for a hydride transfer mechanism of catalysis in Phosphoglucose isomerase from Pyrococcus furiosus, J. Biol. Chem. 278 (47) (2003) 47261–47268.
- [10] D. Arsenieva, et al., The crystal structure of rabbit phosphoglucose isomerase complexed with 5-phospho-arabinonohydroxamic acid, Proc. Natl. Acad. Sci. 99 (9) (2002) 5872–5877.

- [11] J.E.D. Dyson, E.A. Noltmann, The effect of pH and temperature on the kinetic parameters of Phosphoglucose isomerase: participation of histidine and lysine in a proposed dual function mechanism, J. Biol. Chem. 243 (7) (1968) 1401–1414.
- [12] C.J. Jeffery, R. Hardré, L. Salmon, Crystal structure of rabbit Phosphoglucose isomerase complexed with 5-Phospho-d-Arabinonate identifies the role of Glu357 in catalysis, Biochemistry 40 (6) (2001) 1560–1566.
- [13] A.T. Cordeiro, et al., Crystal structure of human phosphoglucose isomerase and analysis of the initial catalytic steps, Biochim. Biophys. Acta 1645 (2) (2003) 117–122.
- [14] S.A. Lesley, et al., Structural genomics of the Thermotoga maritima proteome implemented in a high-throughput structure determination pipeline, Proc. Natl. Acad. Sci. 99 (18) (2002) 11664.
- [15] J.M. Logsdon, D.M. Faguy, Evolutionary genomics: Thermotoga heats up lateral gene transfer, Curr. Biol. 9 (19) (1999) R747–R751.
- [16] T. Hansen, C. Urbanke, P. Schönheit, Bifunctional phosphoglucose/ phosphomannose isomerase from the hyperthermophilic archaeon Pyrobaculum aerophilum, Extremophiles 8 (6) (2004) 507–512.
- [17] F. Rigoldi, et al., Review: engineering of thermostable enzymes for industrial applications, APL Bioeng. 2 (1) (2018), 011501.
- [18] E.F. Pettersen, et al., UCSF chimera—a visualization system for exploratory research and analysis, J. Comput. Chem. 25 (13) (2004) 1605–1612.
- [19] F. Armougom, et al., Expresso: automatic incorporation of structural information in multiple sequence alignments using 3D-Coffee, Nucleic Acids Res. 34 (suppl_2) (2006) W604–W608.
- [20] X. Robert, P. Gouet, Deciphering key features in protein structures with the new ENDscript server, Nucleic Acids Res. 42 (W1) (2014) W320–W324.
- [21] H.E. Klock, S.A. Lesley, The Polymerase Incomplete Primer Extension (PIPE) method applied to high-throughput cloning and site-directed Mutagenesis, in: S. A. Doyle (Ed.), High Throughput Protein Expression and Purification: Methods and Protocols, Humana Press, Totowa, NJ, 2009, pp. 91–103.
- [22] E.A. Noltmann, C.J. Gubler, S.A. Kuby, Glucose 6-Phosphate Dehydrogenase (Zwischenferment): I. Isolation of the crystalline enzyme from yeast, J. Biol. Chem. 236 (5) (1961) 1225–1230.
- [23] A. Grosdidier, V. Zoete, O. Michielin, SwissDock, a protein-small molecule docking web service based on EADock DSS, Nucleic Acids Res. 39 (2011) W270–W277. Web Server issue.
- [24] M.K. Swan, et al., Structural basis for Phosphomannose isomerase activity in Phosphoglucose isomerase from Pyrobaculum aerophilum: a subtle difference between distantly related enzymes, Biochemistry 43 (44) (2004) 14088–14095.
- [25] F. Sánchez-Viesca, R. Gómez, Reactivities Involved in the Seliwanoff Reaction, 2018.
- [26] C.-C. Chou, et al., The crystal structure of Phosphoglucose isomerase/autocrine motility factor/Neuroleukin complexed with its carbohydrate phosphate inhibitors suggests its substrate/receptor recognition, J. Biol. Chem. 275 (30) (2000) 23154– 23160.
- [27] H. Yamamoto, H. Miwa, N. Kunishima, Crystal structure of Glucose-6-phosphate isomerase from Thermus thermophilus HB8 showing a snapshot of active dimeric state, J. Mol. Biol. 382 (3) (2008) 747–762.
- [28] D. Mathur, L.C. Garg, Functional phosphoglucose isomerase from mycobacterium tuberculosis H37Rv: rapid purification with high yield and purity, Protein Expr. Purif. 52 (2) (2007) 373–378.
- [29] L.-C. Sun, et al., Glucose-6-phosphate isomerase is an endogenous inhibitor to myofibril-bound serine proteinase of crucian carp (Carassius auratus), J. Agric. Food Chem. 57 (12) (2009) 5549–5555.
- [30] M.K. Gaitonde, E. Murray, V.J. Cunningham, Effect of 6-Phosphogluconate on Phosphoglucose isomerase in rat brain in vitro and in vivo, J. Neurochem. 52 (5) (1989) 1348–1352.
- [31] M. Meng, et al., Functions of the conserved anionic amino acids and those interacting with the substrate phosphate group of phosphoglucose isomerase, FEBS Lett. 499 (1) (2001) 11–14.
- [32] J.M. Berrisford, et al., Crystal structure of Pyrococcus furiosus Phosphoglucose isomerase: implications for substrate binding and catalysis, J. Biol. Chem. 278 (35) (2003) 33290–33297.
- [33] Francisco Sánchez-Viesca, Reina Gómez, Reactivities Involved in the Seliwanoff Reaction, Modern Chemistry 6 (1) (2018) 1–5, https://doi.org/10.11648/j. mc.20180601.11.
- [34] A. Nakamura, et al., "Newton's cradle" proton relay with amide-imidic acid tautomerization in inverting cellulase visualized by neutron crystallography, Sci. Adv. 1 (2015), e1500263, https://doi.org/10.1126/sciadv.1500263.
- [35] R.K. Chaturvedi, G.L. Schmir, The hydrolysis of N-substituted acetimidate esters, J. Am. Chem. Soc. 90 (16) (1968) 4413–4420.
- [36] T.C. Pletcher, S. Koehler, E.H. Cordes, Mechanism of hydrolysis of N-methylacetimidate esters, J. Am. Chem. Soc. 90 (25) (1968) 7072–7076.